# THE USE OF OPENFOAM AS A VIRTUAL LABORATORY TO SIMULATE OSCILLATING WATER COLUMN WAVE ENERGY CONVERTERS

**I. SIMONETTI**[*1]**, L. CAPPIETTI**[*2]**, H. EL SAFTI**[+3]**, G. MANFRIDA**[†]**, H. MATTHIES**[#]**, H. OUMERACI**[+4]

[*] Dept. of Civil and Environmental Engineering, University of Florence, Florence, Italy
[1] e-mail: irene.simonetti@dicea.unifi.it
[2] e-mail: lorenzo.cappietti@dicea.unifi.it

[†] Dept. of Industrial Engineering, University of Florence, Florence, Italy
e-mail: giampaolo.manfrida@unifi.it

[#] Institute of Scientific Computing, Technische Universität Braunschweig, Brunswick, Germany
e-mail: wire@tu-bs.de

[+] Dept. of Hydromechanics and Coastal Engineering, Technische Universität Braunschweig, Brunswick, Germany
[3] e-mail: h.el-safti@tu-braunschweig.de
[4] e-mail: h.oumeraci@tu-braunschweig.de

**Key words:** Computational Methods, Marine Engineering, Wave Energy Converters, Oscillating Water Column

**Abstract.** The Oscillating Water Column is one of the oldest concepts for wave energy harvesting. The device optimization is still a crucial point for the commercial-scale diffusion of this technology. Therefore, research at fundamental level is still required. The implementation and the application a CFD code for the conduction of a parameter study aiming at the optimization of the device is presented. The numerical set up and the validation of a virtual wave flume in the open-source environment OpenFOAM® are initially presented, using comparatively different wave generation approaches. The application of the model to simulate the device and a validation with physical results are shown. The model solves incompressible 3D Navier-Stokes equations for a single Eulerian fluid mixture of water and air, using a Finite Volume Method for equations discretization and the Volume Of Fluid method for free surface tracking. Different turbulence models are tested, comparing their suitability for this particular application both in terms of computational cost and model capability to reproduce the experimental data.

## 1 INTRODUCTION

The Oscillating Water Column (OWC) wave energy converter, at a basic concept level, consists in a pneumatic chamber, open below the water level. The air trapped above the inner water surface and the pressure variation due to the wave-induced water oscillation inside the

chamber produces an airflow through a duct, which drives a self-rectifying turbine [1-2].

The hydrodynamics in terms of resonance, diffraction and radiation problems around the structure is the most analysed aspect in the field of OWC modelling. The aerodynamics inside the air chamber and ducts is usually modelled by using mass conservation principles and the approximation of isentropic compression/decompression processes in the air chamber.

The linear wave theory has traditionally been applied to study the interaction between incident waves and OWCs, with the application of simplified models such as the rigid piston model [3-6] and the uniform pressure distribution model [7-8]. When the OWC geometry is complex, or a relevant effect of the installation site bathymetry is expected, Finite Element Methods (FEM) or Boundary Element Methods (BEM) [9-11] are usually applied to compute the OWC hydrodynamic coefficients of added mass and radiation damping.

When a proper characterization of viscous effects due to boundary layer separation, wave breaking and turbulence are expected to be relevant, approaches based on potential flow theory are no longer appropriate, and a solution based on Navier-Stokes equations (Computational Fluid Dynamic, CFD) is required. However, the hydrodynamics and aerodynamics of the two-phase system are currently not yet included in studies using a CFD approach.

The present study focuses on the application of CFD to the numerical modelling of a three-chamber OWC device and on the comparison of numerical results with data from physical tests. The initial development stages of an air-water model of hydrodynamic and aerodynamic processes related to OWC devices are presented. The main emphasis of the paper is to compare the performance of different wave generation approaches and turbulence models in terms of their capability to reproduce the relevant phenomena for the specific case of interest.

In section 2, the theoretical background of the CFD numerical model is summarized, along with some theoretical details on the turbulence models applied in this work. The different wave generation approaches for the numerical wave flume are presented and compared in section 3. In section 4, the set up of a 3D numerical model of the OWC device is presented, as well as a comparison between numerical and physical model results. The effect of the use of different turbulence model on the simulation results is also presented in this section.

## 2 NUMERICAL MODEL IN OPENFOAM: THEORETICAL BACKGROUND

The study is carried out using the *interFoam* solver within the OpenFOAM® framework. It solves for the incompressible 3D Navier-Stokes equations for a single Eulerian fluid mixture of two-phases (i.e. water and air). The discretization of the flow equations is based on the Finite Volume Method (FVM) with a co-located methodology for unstructured polyhedral meshes with arbitrary grid elements (fluids quantities are stored at control volume centroids). The Volume Of Fluid (VOF) method is used for free surface tracking [12].

### 2.1 Governing equations

Considering a Newtonian, homogeneous, incompressible and isothermal fluid, the set of governing equations for fluid dynamics are the mass and momentum balance equations (Eqs 1-2):

$$\nabla \cdot \mathbf{u} = 0 \tag{1}$$

$$\frac{\partial(\rho\mathbf{u})}{\partial t} + \nabla\cdot(\rho\mathbf{u}\mathbf{u}) = -\nabla p + \nabla\cdot\mathbf{T} + \rho\mathbf{f}_b \tag{2}$$

where $\mathbf{u}$ is the fluid velocity field, $\rho$ is the fluids density, $p$ is the pressure, $\mathbf{T}$ is the deviatoric viscous stresses tensor and $\mathbf{f}_b$ are the body forces per unit of mass. Introducing the volume phase fraction $\gamma$ (with $0 \le \gamma \le 1$ and values 0 and 1 for the regions containing respectively only air or only water), the transport equation for $\gamma$ is:

$$\frac{\partial\gamma}{\partial t} + \nabla\cdot(\mathbf{u}\gamma) = 0 \tag{3}$$

If the contributions of liquid and gas velocities to the free surface evolution are assumed proportional to their volume fractions, the effective fluid velocity is defined through a weighted average

$$\mathbf{u} = \gamma\mathbf{u}_l + (1-\gamma)\mathbf{u}_g \tag{4}$$

where l, g denotes liquid and gas fractions respectively. Introducing the relative velocity vector $\mathbf{u}_r = \mathbf{u}_l - \mathbf{u}_g$, the transport equation for $\gamma$ can be defined as

$$\frac{\partial\gamma}{\partial t} + \nabla\cdot(\mathbf{u}\gamma) + \nabla\cdot(\mathbf{u}_r\gamma(1-\gamma)) = 0 \tag{5}$$

where $\mathbf{u}_r$ is an artificial contribution to the phase fraction convection to prevent the interface from smearing. In *interFoam*, therefore, the classic VOF approach is modified in order to improve boundedness and conservativeness of $\gamma$.

The Multidimensional Universal Limiter with Explicit Solution (MULES) of OpenFOAM® is used in the solution procedure to ensure boundedness of the phase fraction.

The hybrid PISO-SIMPLE algorithm (PIMPLE) is used for the pressure-velocity system equation coupling. The PIMPLE algorithm provides the solver the ability to solve steady states as well as transient problems with larger time steps.

## 2.2 Turbulence modeling

In OpenFOAM®, turbulence modeling is generic: incompressible CFD solvers may perform direct numerical simulations (DNS) (i.e. without any turbulence modeling), Large Eddy Simulations (LES), Detached Eddy Simulations (DES) or solve Reynolds-averaged Navier-Stokes (RANS) with different turbulence model closures.

In the present work, a *k-ω SST* (Shear Stress Transport) turbulence model in RANS framework and a LES model were comparatively tested. The *k-ω SST* turbulence model is a two-equation eddy-viscosity model which combines the *k-ω* and the *k-ε* models: a blending function activates the *k-ω* model near the wall and the *k-ε* model in the free stream.

The Large Eddy Simulation (LES) here applied uses a k-equation eddy-viscosity model (*oneEquationEddy* in OpenFOAM®). In this model, a transport equation for the sub-grid scale (SGS) turbulent kinetic energy $k_{SGS}$ is introduced and solved, to take into account the effects of convection, diffusion, production and destruction on the SGS velocity scale [13]. The transport equation solved for $k_{SGS}$ is

$$\frac{\partial(\rho k_{SGS})}{\partial t} + \nabla\cdot(\rho k_{SGS}\mathbf{u}) = \nabla\cdot\left((\mu_{SGS}+\mu)\nabla k_{SGS}\right) + 2\mu_{SGS}S_s^2 - \rho\frac{C_\varepsilon k_{SGS}^{2/3}}{\Delta} \tag{6}$$

where $\Delta$ is the spatial filter size (separating the resolved eddies from the SGS ones, which are modeled), $C_\varepsilon = 1.048$ is the model constant, $S_S$ is the strain rate tensor magnitude, $\mu$ is the

laminar viscosity and $\mu_{SGS}$ is the SGS viscosity calculated as

$$\mu_{SGS} = C_{SGS}\Delta\sqrt{k_{SGS}} \tag{7}$$

with the constant $C_{SGS} = 0.01$ [13].

## 3 NUMERICAL WAVE FLUME

Two wave generation approaches were preliminary tested and compared, in order to highlight the strength and the drawbacks of two methods in terms of both accuracy on reproducing the wave dynamics and computational demands.

### 3.2 Wave generation with *waves2Foam* toolbox

The *waves2Foam* toolbox [14] is implemented within the *interFoam* hydrodynamic solver for generation/absorption of waves. The hydrodynamic solver is coupled with a relaxation zones approach. At the domain inlet, a boundary condition is defined to introduce waves according to different wave theories. Inside the relaxation zones the required wave profile are defined: velocity components and wave surface elevation are imposed using a relaxation function (Eq. 8).

$$\alpha_R = 1 - \frac{e^{\left(\chi_R^{3.5}\right)} - 1}{e^{(1)} - 1} \tag{8}$$

The relaxation function is applied to impose the values of $\gamma$ and $\mathbf{u}$ to generate and/or to absorb waves at each time step (Eq. 9).

$$\Phi = \alpha_R \Phi_{computed} + (1 - \alpha_R)\Phi_{target} \tag{9}$$

where $\Phi$ indicates either $\gamma$ or $\mathbf{u}$, $\chi_R$ is defined to have $\alpha_R = 1$ at the end of the relaxation zone. In the outlet relaxation zone, $\gamma_{target}$ is determined based on the still water level (SWL).

### 3.1 Wave generation with a piston-type wave maker

A piston-type wave maker was numerically simulated to accurately mimic the way waves are generated in the physical wave flume available at the laboratory of maritime engineering LABIMA of the University of Florence. The piston wave maker was simulated imposing a moving wall boundary condition, causing the mesh to change with every time step (i.e., a dynamic mesh was adopted). The time history of positions of the wave maker can be given as an input to impose a prescribed motion to the numerical piston wave maker.

To accommodate this motion in the framework of OpenFOAM® FVM discretization, the Laplace equation (Eq. 10) is solved, using a vertex-based solution method to determine the positions of internal points in the mesh (Eq. 11), based on the prescribed boundary motion of the piston [15-16].

$$\nabla \cdot (\varsigma\nabla\mathbf{v}) = 0 \tag{10}$$

$$x_{new} = x_{old} + \mathbf{v}\Delta t \tag{11}$$

where $\varsigma$ is a diffusion field, $\mathbf{v}$ is the velocity used to modify the internal point position; $x_{new}$ and $x_{old}$ are the point positions after and before mesh adjustment across the time step $\Delta t$.

A distance-based diffusivity ς was applied to the Laplace equation (i.e. the diffusivity field is a function of the cell distance from the moving boundary) to calculate the displacement of each point in the computational domain.

For wave absorption, a relaxation zone was placed at the outlet of the domain, hence using the same concept used in *waves2Foam* toolbox for wave absorption (Fig. 1).

### 3.3 Comparison of wave generation approaches

The two wave generation approaches were tested by comparing wave propagation along empty numerical wave flumes with data from physical tests, for both 2D and 3D cases. A reference regular wave having height H = 0,063 m and period T = 1.1 s on a 0.5 m still water level (SWL) was used to perform the comparison. The simulation domains have a length of 15 m (Fig. 1), with 2 m inlet and outlet relaxation zones for wave generation/absorption used for the *waves2Foam* approach, and a 2 m outlet relaxation zone for wave absorption used in the piston wave maker generation approach (hence, the length of the relaxation zones is approximately 1.12 times the reference wave length λ). It is worth to note that the physical flume is 37 m long while the numerical counterpart was reduced to 15 m in order to save computational time. The time-window for data analysis was chosen in order to exclude the effect of any possible, although limited, wave reflection from the end of the virtual flume.

For wave generation with *waves2Foam*, a Stokes second order wave theory boundary condition was used. For the piston wave maker, the time history of positions of the moving boundary recorded in the physical test was used as an input, in order to prescribe exactly the same motion of the physical and numerical wave makers.

Three wave gauges (WGs) are placed along the wave flume to obtain the time series of the free surface displacement η. The WGs used in the physical tests are ultrasonic sensors with a declared accuracy of ±1mm.
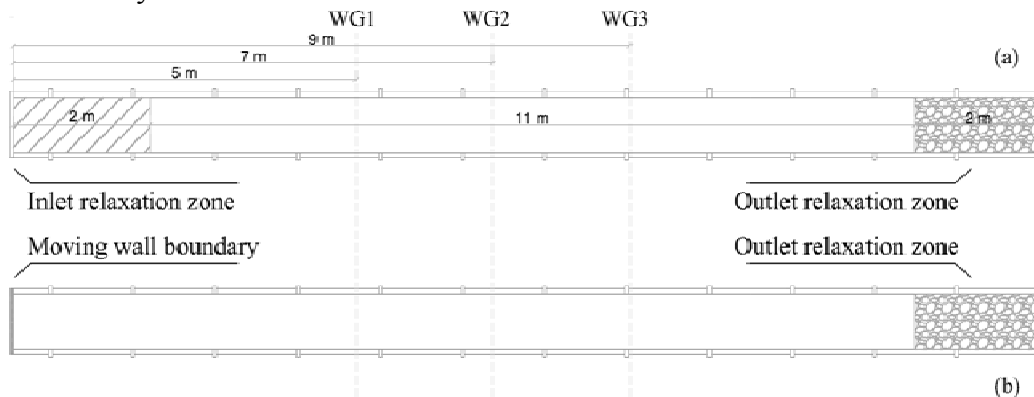


**Figure 1:** Sketch of the simulation domain for the numerical wave flumes with *waves2Foam* approach (a) and piston wave maker (b) wave generation approaches.

The relative error between simulated and physical data was calculated for η and T at the different WGs. In the fully developed wave field, a good agreement was found for the considered WGs for both *waves2Foam* and piston wave generation approaches, with a maximum relative error lower than 10% on η (Tab. 1) and 1% on T. The relative error of the η simulation with the piston wave maker is ~2% lower than the one obtained with *waves2Foam* generation. Considering the accuracy of the WGs used in physical tests for the

measurements of the wave profile, the agreement between the numerical results and the physical measurements is considered very good. In the region where the wave field is not fully developed (i.e. before ~ 5 wave periods from the moment of the first wave arrival at the reference WG), however, remarkable differences in η are noticed in the case of *waves2Foam* generation (Fig. 2): the first free surface displacement takes place about two wave periods earlier than the first wave arrival for experimental and piston wave-maker generation, and the surface profile develops faster. This effect, due to the specific initial paddle displacement of the wave maker, does not produce remarkable differences in the fully developed wave field.

**Table 1:** Maximum relative error on η between simulated and physical data at wave gauges WG1, WG2 and WG3 for generation with *waves2Foam* and Piston wave maker, computed for the fully developed wave field.

| | Maximum relative error on η [%] | |
|---|---|---|
| | *wave2Foam* | Piston wave maker |
| WG1 | ~ 6 | ~ 4 |
| WG2 | ~ 9 | ~ 7 |
| WG3 | ~ 9 | ~ 8 |
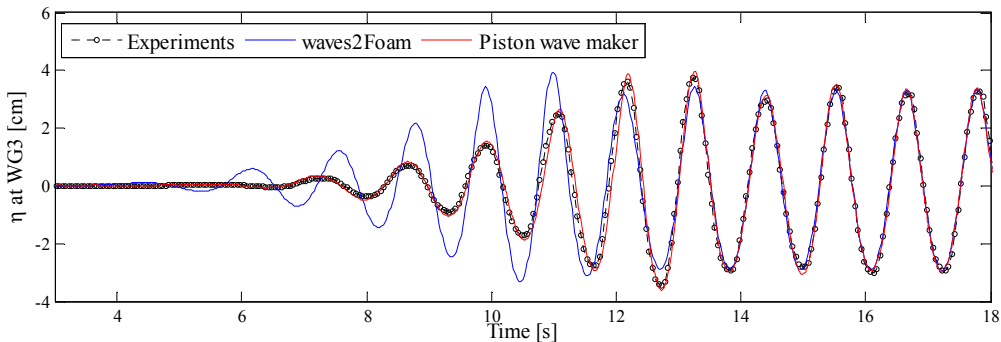


**Figure 2:** Comparison between physical and numerical water surface elevation displacement time series at wave gauge WG3 (9 m from wave generation) for a monochromatic wave with H = 6.3 cm and T = 1.1 s.

The computational time needed to complete a 30 s simulation on a single 2.3 GHz processor equipped with 8 Gb of RAM memory is about 2 hours for the *waves2Foam* generation, while about 6 hours are necessary for the piston wave-maker generation. The higher computational time is related to the application of the dynamic mesh.

## 4   3D MODEL OF THE OSCILLATING WATER COLUMN DEVICE

A 3D model of the OWC was developed in OpenFOAM® in order to reproduce more accurately than in the 2D code the complex dynamics that emerge from the wave-OWC interaction in the near field. The simulated device consists of three identical rectangular-shaped chambers, each equipped with a circular vent on the top cover, to mimic the presence of the turbine by introducing a pressure drop. The circular shape of the vent is adopted to introduce a quadratic air flow-pressure relation, which is typical for impulse turbine, e.g. the biradial turbine proposed by Fãlcao [17].

The simulated OWC geometry corresponds closely to that tested in the LABIMA flume

[18].

The *Waves2Foam* wave generation approach was used in all subsequent simulations, in order to reduce the computational demands of the 3D model.

## 4.1  Simulated geometry and discretization

Each of the three simulated OWC chambers (Fig. 4) is 0.1 m wide in the wave propagation direction, with a fixed capture width of 0.2 m, a back wall length of 0.45 m, a front wall draught of 0.11 m and a freeboard level of 0.15 m. The diameter of the top cover vent is set to 0.022 m. The values chosen for the dimensions of the tested OWC were selected considering the literature review, the dimensions of built full scale prototypes [2-3], and the preliminary results of a parametric simplified frequency domain model [19].

The computational domain has a length of 5.5 meters (3.5 m before and 2 m after the OWC structure), a height of 0.7 meters and a width of 0.8 meters (corresponding to the width of the used physical wave-current flume). Inlet and outlet relaxation zones have a length of 1 m each. The SWL is set to 0.5 m.

A 3D model of the OWC geometry was generated in STereoLithography (STL) format using the open source three-dimensional finite element mesh generator Gmsh [20]. Then, a hexahedra-predominant mesh for the whole simulation domain was created using the OpenFOAM® mesh generator *snappyHexMesh*. The mesh is refined in specific regions (Fig. 3), particularly: around the expected free surface and the OWC front wall zone (where flow separation may happen); around the OWC structure; around the top cover vent and pipe. In the free surface zone, the mesh size is selected based on the incident wave properties, so that mesh resolution is not lower than 6 cells per wave height $H$ and 78 cells per wave length $\lambda$. Around the vent and the pipe, a fine mesh is adopted to properly discretize the cylindrical geometry: about 6 cells per vent diameter are used. The resulting mesh has a size of about 550'000 cells.

The mesh quality was controlled in *snappyHexMesh* by setting the appropriate number of iteration for each mesh generation step (e.g. snapping to the surface, layer adding) and imposing maximum allowable values for mesh quality parameters. The final mesh, composed of hexahedra and polyhedral exclusively, has maximum and average non orthogonal degree of 55.7 and 9.3 respectively, and a maximum skewness of 2.8.
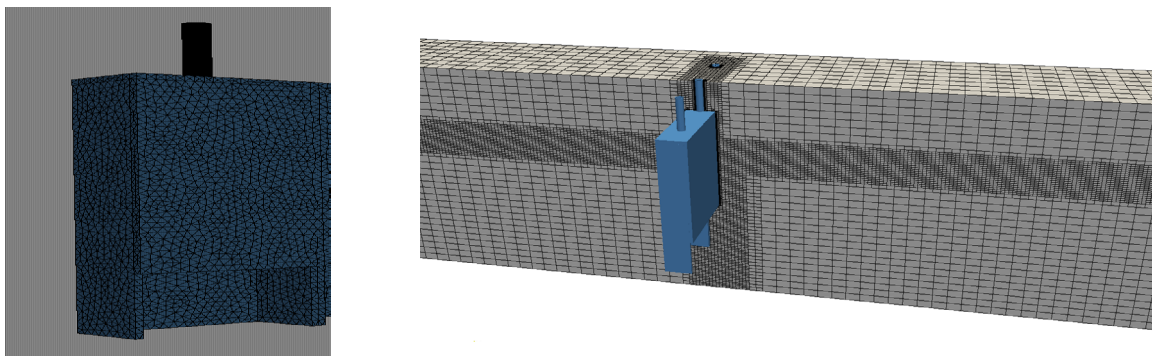


**Figure 3:** Three chambers OWC device geometry generated in STL format (left) and detail of the computational mesh in the OWC near field with a cross-section view on the symmetry plane (right).

## 4.2  Numerical model set up

No slip boundary conditions are used at the bottom of the numerical wave flume and on the OWC walls, while the water surface is set as a constant atmospheric pressure boundary. Velocity components and water surface elevations at inlet relaxation zone are defined to introduce regular waves with *waves2Foam* toolbox, using a Stokes second order wave theory.

Time derivatives are discretized by using a first-order implicit Euler scheme. A standard finite volume discretization of Gaussian integration is applied to gradient operators, with a central differencing scheme for cell centre to cell face value interpolation. The convection term in the momentum equation is discretized with a central difference interpolation scheme. For the convection term in the phase fraction $\gamma$ transport equation, the Monotone Upwind Scheme for Scalar Conservation Laws (MUSCL) [21] interpolation scheme is used. The linear solver used for the solution of the discretized equation systems is a generalized geometric-algebraic multi-grid solver (GAMG) with a simplified diagonal based incomplete Cholesky (DIC) smoother.

A self-adjusting time step $\Delta t$ is applied to increase the stability of the solution procedure. $\Delta t$ is adapted at the beginning of every new time loop according to the given maximum value of the Courant number C, fixed to 0.6.

Two different turbulence models were tested:  *k-$\omega$ SST* (RANS framework) and a k-equation eddy-viscosity Large Eddy Simulation (LES). In the *k-$\omega$ SST* model, wall functions are applied as boundary conditions on the OWC structure and on the wave flume bottom and lateral walls, to model near wall turbulence.

## 4.3  Effect of turbulence modeling and comparison with physical test data

A reference regular wave having height H = 0.04 m and period T = 1 s on a 0.5 m still water level (SWL) was used for preliminary testing of the OWC 3D model and for comparing the performances of the two turbulence models adopted.

Values of the surface elevation, $\eta_{OWC}$, and air pressure, P, were sampled inside the central OWC chamber (Fig. 5-6). Time series of vertical component of the air velocity, U, were sampled inside the pipe equipping the circular vent on the top cover of the central chamber (Fig. 8). The relative error between numerical results and data from physical testing was computed (Tab. 2).
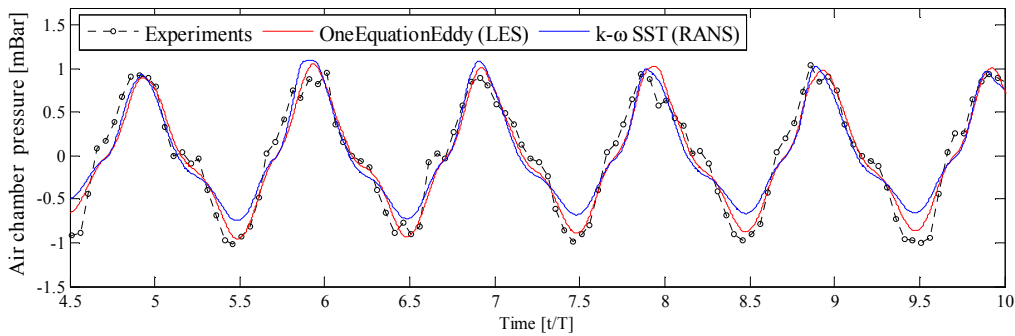
For $\eta_{OWC}$, the maximum relative error between numerical and experimental is about 5% for the k-equation eddy-viscosity LES turbulence model and about 15% for the *k-$\omega$ SST* turbulence model. In particular, a higher water oscillation inside the OWC is observed when the RANS model is used, which may indicate that the model fails to accurately predict fluid viscosity effects and the flow separation taking place in the proximity of the OWC front wall (Fig. 9), hence it underestimates the associated vortex flow energy losses.

For the air chamber pressure *p*, and the air velocity in the pipe $u_y$, a good agreement was found between numerical and experimental data (i.e. the maximum relative error is lower than 10% for both parameters) when using the k-equation eddy-viscosity LES turbulence model. Also in these cases, a bigger deviation (~ 20% of relative error) was found when using the *k-$\omega$ SST* turbulence model, coherently with the deviation observed in the simulation of the water column oscillation $\eta_{OWC}$.
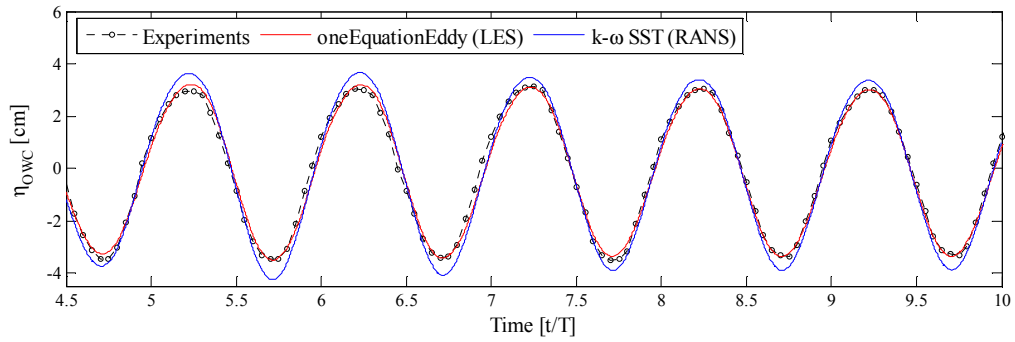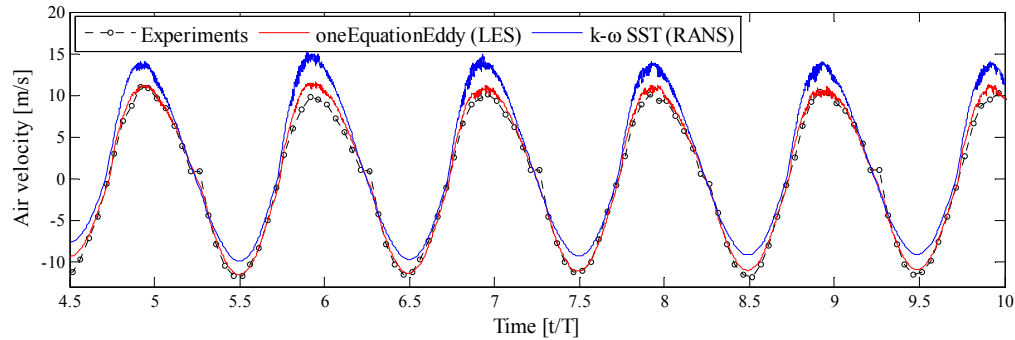
**Figure 3:** Comparison between experimental and numerical (with k-equation eddy-viscosity LES and *k-ω SST* turbulence model) results for water surface oscillation $\eta_{OWC}$ in the OWC chamber.



**Figure 4:** Comparison between experimental and numerical (with k-equation eddy-viscosity LES and *k-ω SST* turbulence model) results for air chamber pressure *p* in the OWC chamber.



**Figure 5:** Comparison between experimental and numerical (with k-equation eddy-viscosity LES and *k-ω SST* turbulence model) results for vertical air velocity $u_y$ in the OWC pipe.

**Table 2:** Relative error between numerical and experimental data ($\eta_{OWC}$, $T_{OWC}$, *p*, $u_y$) for the 3D OWC model with k-equation eddy-viscosity LES and *k-ω SST* turbulence model.

| | Maximum relative error [%] | | | |
|---|---|---|---|---|
| | $\eta_{OWC}$ | $T_{OWC}$ | *p* | $u_y$ |
| oneEqationEddy | ~ 5 | < 1 | ~ 7 | ~ 7 |
| k-ω SST | ~ 15 | < 1 | ~ 20 | ~ 20 |

Limited differences on computational time were observed using the two turbulence models: the computational time needed to complete a 10 s simulation with a parallel run on four 2.3 GHz processors is about 40 hours when using the *k-ω SST* turbulence model, and it increases of about 15% for the k-equation eddy-viscosity LES.

It has to be noted, however, that the higher air velocities predicted in the pipe using the *k-ω SST* turbulence model (up to 15 m/s, against maximum values of around 12 m/s for the k-equation eddy-viscosity LES) imply the use of a smaller time step to satisfy the Courant number criteria, thus increasing the computational cost of the RANS simulation.
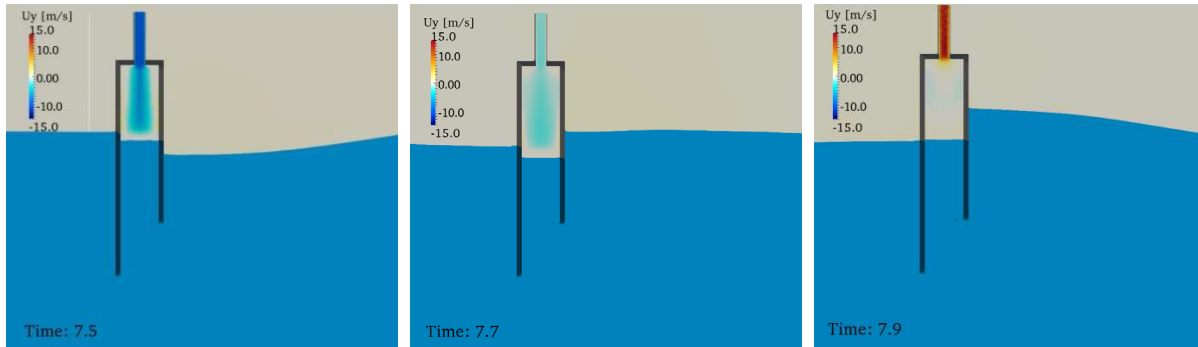


**Figure 6:** 2D cross-section of vertical component of the air velocity in OWC central chamber and water surface elevation levels at different time steps during wave propagation, simulated with k-equation eddy-viscosity LES turbulence model.
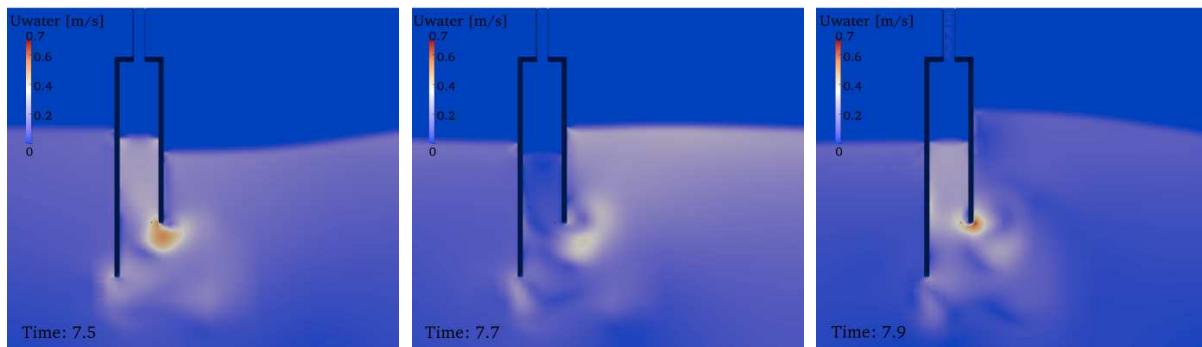


**Figure 7:** 2D cross-section of water velocity near the OWC central chamber at different time steps during wave propagation, simulated with k-equation eddy-viscosity LES turbulence model.

## SUMMARY AND CONCLUDING REMARKS

In this work, the use of OpenFOAM® CFD for the numerical simulation of a three-chamber OWC device was tested. Results were compared with experimental data from physical tests performed on the wave-current flume of Florence University (www.labima.unifi.it). The numerical set up of both the numerical wave flume and the specific 3D OWC model was presented.

Two wave generation approaches were compared: (i) wave generation using *waves2Foam* toolbox and (ii) wave generation with a numerical piston wave-maker based on a dynamic mesh with a moving-wall boundary condition. Both approaches were found to be fairly good in reproducing experimental measured water surface displacement in the completely

developed wave field (i.e. relative errors lower than 10%). The numerical piston wave maker, however, permits a more accurate simulation of the wave motion and thus a more coherent comparison between numerical and experimental results for model validation purposes.

Results of the 3D model of the OWC devices, tested in regular waves by using *waves2Foam* toolbox, are in good agreement with experimental data (relative error lower than 7% for all the considered benchmark parameters) using a k-equation eddy-viscosity Large Eddy Simulation. A higher deviation from experimental data was found using a *k-ω SST* turbulence model, which may reflect a worse prediction of viscosity effects and the flow separation taking place in the proximity of the OWC front wall.

## ACKNOWLEDMENTS

## REFERENCES

[1]  Boake, C.B., Whittaker, T.J.T., Folley, M., Ellen, H. Overview and Initial Operational Experience of the LIM-PET Wave Energy Plant. *Proceedings of the 12th Int. Offshore Polar Eng. Conference* (2002).

[2]  Torre-Enciso, Y., Ortubia, I., De Aguileta, L.I.L., Marqués, J. Mutriku Wave Power Plant: from the thinking out to the reality. *Proceedings of the 8th Eur. Wave Tidal Energy Conf., Uppsala, Sweden.* (2009).

[3]  Evans, D.V. *The Oscillating water Column Wave Energy Device*. J. Fluid Mechanics 22 (1978) pp: 423-433.

[4]  Lopes, M.F.P. Hals, J. Gomes, R.P.F. Moan, T., Gato, L.M.C., Falcão, AF de O. 2009. *Experimental and numerical investigation of non-predictive phase-control*. Ocean Eng. 36 (2009) pp: 386–402.

[5]  Falcão, A.F. de O., Henriques, J.C.C., Candido, J.J. *Dynamics and optimization of the OWC spar buoy wave energy converter*. Renewable energy 48 (2012) pp: 369-381.

[6]  Karami, V., Ketabdari, M.J., Akhtari, A.K. *Numerical modelling of the oscillating water column wave energy convertor*. Int. J. Advanced Renewable Energy Research. 1 (2012) pp: 196-206.

[7]  Brendmo, A., Falnes, J., Lillebekken, P.M. *Linear modelling of oscillating water columns including viscous loss*. Applied Ocean Research 18 (1996) pp: 65-75.

[8]  Falcão, A.F. de O., Justino, P.A.P. *OWC Wave energy devices with air-flow control*. Ocean Engineering 26 (1999) pp: 1275-1295.

[9]  Brito-Melo, A., Hoffman, T., Sarmento, A.J.N.A., Clément, H., Delhommeau, G. *Numerical modelling of OWC-shoreline devices including the effect of surrounding coastline and non-flat bottom*. Int. J. offshore Polar Eng. 11 (2001) pp: 147-154.

[10] Delauré, Y.M.C. & Lewis, A. *A 3D hydrodynamic modeling of a fixed oscillating water column wave power plant by a boundary element methods*. Ocean Engineering 30 (2003) pp: 309-330.

[11] Josset, C. & Clément, A.H. *A time-domain numerical simulator for oscillating water column wave power plants*. Renewable Energy 32 (2007) pp: 1379-1402.

[12] Hirt C. & Nichols B. *Volume of fluid (VOF) method for the dynamics of free boundaries*. J. Comput. Phys. 39 (1981) pp: 201–225.

[13] Villers, E. *The Potential of Large Eddy Simulation for the Modeling of Wall Bounded Flows*. PhD thesis. Imperial College of Science, Technology & Medicine (2006).

[14] Jacobsen N.G., Fuhrman D.R., Fredsøe J. *A wave generation toolbox for the open-source CFD library : Open-Foam. Int. J. Num. Methods Fluids* 70 (2012) pp: 1073–88.

[15] Jasak, H. and Tukovic, V. *Automatic mesh motion for the Unstructured Finite Volume Mehod*. Transaction of FAMENA, Vol. 30, 2 (2007) pp. 1-8.

[16] Jasak, H. Dynamic Mesh Handling in OpenFOAM applied to Fluid Structure Interaction simulations. *Proceedings of 5th European Conference on Computational Fluid Dynamics ECCOMAS CFD* (2010) 19 pp.

[17] Falcão, A.F. de O., Gato, L.M.C., Nunes, E.P.A.S. *A novel radial self-rectifying air turbine for use in wave energy converters. Part 2. Results from model testing*. Renewable Energy 53 (2013) pp: 159-164.

[18] Crema, I., Cappietti, L., Simonetti, I., Oumeraci, H. Laboratory Experiments on Oscillating Water Column wave energy converters integrated in a Very Large Floating Structure, *Proceedings of 11th European European Wave And Tidal Energy Conference* (2015) submitted.

[19] Simonetti I. Cappietti L., El Safti H., Oumeraci H. Numerical Modelling Of Fixed Oscillating Water Column Wave Energy Conversion Devices: Toward Geometry Hydraulic Optimization, *Proceedings of the ASME 34th International Conference on Ocean, Offshore and Arctic Engineering OMAE2015* (2015) accepted.

[20] Geuzaine, C. *Gmsh: a three-dimensional finite element mesh generator with built-in pre- and post-processing facilities*. Int. J. Numer. Meth. Eng. 0 (2009) pp: 1-24.

[21] Van Leer, B. *Towards the ultimate conservative difference scheme*. J. Comput. Phys. 32 (1979) pp: 101–36.